Advances in Research

Volume 26, Issue 3, Page 48-61, 2025; Article no.AIR.135080
ISSN: 2348-0394, NLM ID: 101666096

Effect of Alkaline Earth Metal Doping on Photocatalytic Behaviour of Lanthanum Manganite Perovskite Nanoparticles for Degradation of Organic Pollutants

Himansulal Nayak [a*]

[a] P.G. Department of Chemistry, Orissa University of Agriculture and Technology, Bhubaneswar- 751003, Odisha, India.

Author's contribution

The sole author designed, analyzed, interpreted and prepared the manuscript.

Article Information

DOI: https://doi.org/10.9734/air/2025/v26i31324

Open Peer Review History:
This journal follows the Advanced Open Peer Review policy. Identity of the Reviewers, Editor(s) and additional Reviewers, peer review comments, different versions of the manuscript, comments of the editors, etc are available here: https://pr.sdiarticle5.com/review-history/135080

Original Research Article

Received: 20/02/2025
Accepted: 25/04/2025
Published: 29/04/2025

ABSTRACT

Lanthanum manganite doped with calcium,barium and strontium having perovskite structures (LCMO, LBMO and LSMO) have been prepared through sol-gel technique and characterized by XRD, FTIR, ICP-AES, SEM, EDX and UV-VIS spectroscopy. The XRD data showed the formation of single crystalline phases. SEM images showed that the micro sized structure with average diameter of 1-5 µm. The ICP-AES and EDX data confirmed the formation of required stoichiometric $La_{1-x}M_xMnO_3$ Oxide. Metal doping resulted in reduction of band gap energy (E_g) of the Lanthanum Manganite whose catalytic performance towards photodegradation of Methylene Blue (MB) dye was

**Corresponding author: E-mail: himansu110@gmail.com;*

Cite as: *Nayak, Himansulal. 2025. "Effect of Alkaline Earth Metal Doping on Photocatalytic Behaviour of Lanthanum Manganite Perovskite Nanoparticles for Degradation of Organic Pollutants". Advances in Research 26 (3):48-61. https://doi.org/10.9734/air/2025/v26i31324.*

evaluated using visible light of constant dose for several hours at pH value 4. The results showed highest photocatalytic efficiency 68.52 % in case of LCMO in 100 min illumination time. For LBMO and LSMO the values were 47.92 and 54.87% respectively. But the pseudo first order rate constant 'k'followed the reverse order with highest value in case of LBMO. The linear increase in rate of photodegradation was found to be a function of irradiation time. These findings showed convincingly that $La_{0.7}M_{0.3}MnO_3$[M= Ca, Ba, Sr], possessed great promise for visible light driven photodegadation of MB dye. The reproducibility of the sample for degradation was also studied.

Keywords: Perovskite, sol-gel technique, photocatalyst, methylene blue.

1. INTRODUCTION

Semiconductor photocatalytic processes have been widelyapplied to initiate photocatalytic reactions for the degradationof pollutants. Perovskites type oxides, ABO_3, have been extensively investigated as catalysts for several processes including fuelcells(Tao et al., 2005), water dissociation (Kim et al., 2005), hydrogenation, hydrogenolysis(Ichimura et al., 1992) and ammonia oxidation (Isupova et al., 2005). Nanostructured rare earth manganites doped with alkaline earth metals show interesting electric properties (Kuo and Kai, 2009). Perovskites, especially $LaMnO_3$, have been used in environmental applications e.g. the oxidation of hydrocarbons (Yi et al., 2005, Stephan et al., 2004, Lee et al., 2001), chlorinated organic compounds (Lago et al., 2007) etc. To develop more efficientphotocatalyst, there is an urgent need for photocatalyticsystems,which are able to operate effectively under visible light irradiation.The use of semiconductor photocatalyst under visible light has recentlydrawn much attention. Removal of organic dyes by photocatalyticdegradation is emerging as an effective treatment method. Thepartialsubstitution(doping) of a trivalent rare-earth by the divalent alkaline-earth cations produces a mixed valency of $Mn^{3+}(t_{2g}3\ e_g1)$ and $Mn^{4+}(t_{2g}3\ e_g0)$ ions. It is believed that the doubleexchange (DE) interaction between a pair of these Mn ions is responsible for the electrical and magnetic properties (Khalid et al., 2013).

Nanostructured manganites such as $La_{1-x}Ca_xMnO_3$, $La_{1-x}Sr_xMnO_3$ and $La_{1-x}Ba_xMnO_3$ have been extensively studied in the last decade owing to their notably affected magnetic and electric properties at the nanoscale. The Mn^{4+}/Mn^{3+} ratio strongly depends on the substitution, therefore the classic method used to change the ratio is substituting La^{3+} by Sr^{2+} with different doping levels. When the doping amount of Sr^{2+} is around 0.33 , the ratio of Mn^{4+}/Mn^{3+} is 1:2, which is the optimum ratio for the transport property of the system. Additionally, the number of manganese ions may also be changed by creating oxygen vacancies (oxygen deficiency), leading to the modification of the exchange interactions . The oxygen content is crucial in determining the magnetic and electrical properties of the manganites. Due to the generation of oxygen vacancies, the manganites have technological applications in many fields, such as in solid oxide fuel cells (SOFC), high-temperature electrolyzers, oxygen sensors, and catalyses (Zhou et al., 2018). As variation of A-site cationic radius using alkaline earth metal dopants plays a vital role in determining the various properties of the manganites. By varying the cation, a mismatch occurs between thecation already presented at the A-site (La in the present case) and the dopant cation (Ca, Sr or Ba). This mismatch is expressed in terms of variance might influence the electrical and magnetic properties of manganites.

Over the past decades, photocatalytic oxides or compounds have beenincreasingly utilized in water purification. Manganitesby nature is same as semiconductorshaving an empty conduction band (CB) and a full valence band (VB) in their electronic structure (Kumar et al., 2018). Thus this property; band gap energy, highlights the application of manganites in photocatalytic processes (Barrocas et al., 2016). In the present work, the choice of three specific cations,Ca^{2+},Sr^{2+},Ba^{2+} is based on their similar atomic properties due to their position in the periodic table. In this letter an attempt is made to investigate the effect on the A-site cationic radius $\langle r_A \rangle$by varying the divalent alkaline earth dopants as Ca, Sr and Ba in $LaMnO_3$.

Organic and toxic pollutants pollute water sources indifferent dyeing factories (Sakamoto et al., 2019). Common methods of treatment dyes with a complex aromatic structure can be very difficult to degrade since products resulting from different reactions, such as hydrolysis and oxidation in aqueous media, produce toxicity and carcinogenic substances. These products should be removed with appropriate treatment methods

for publichealth and safety (Gowthami et al., 2018). In recent years,enormous research and development have gained considerable importance as an environmental remediation process in photocatalysis because it can fully remove organic andinorganic toxins from water pollutants by using nanosized metal oxides as catalysts (Guillaume et al., 2018, Kanakaraju and Wong, 2018, Yerkinova et al., 2018). Several metal oxide nanosized semiconductor nanoparticles have been used indifferent applications. The predominant researchin the field of photocatalysis for wastewater purification has included semiconductors of wide band gap and high surface-to-volume ratio material such as titanium dioxide (TiO_2),zinc oxide (ZnO), tin oxide (SnO_2), and zirconium oxide(ZrO_2) (Anandan et al., 2020). These hole-doped compounds play a role in transferring the electronic system to the Fermi level to ensure that conductivity and valence band behaviour is observed.

The coexistence of electrons and holes in manganites introduces them into optical systems as promising materials (Esmaeili et al., 2019). Doped alkaline rare earth transition metal perovskite-like structure oxides reduce the band gap energy values because this feature increases the charge carrier separation (photogenerated electrons and holes) (Ismail et al., 2010). Intense studies were conducted on the materials because their electrical and optical propertiescan be tuned, indicating control of the rational design structure in ABO_3 perovskite by cationic substitutions. So, we can say that perovskite compounds are one of the promising structures that adapt the band gap values to collect the visible-light absorption and the capacity of the band edge to meet the specific photocatalytic needs. The photodegradation of $La_{0.7}Sr_{0.3}MnO_3$ has been achieved up to 99% compared to other samples with high degradation rate under UV lights of wavelength 254 nm. A $La_{0.7}Sr_{0.3}MnO_3$ nanocomposite performs as a photocatalyst to enhance the efficiency of methylene blue photodegradation (Ghozza et al., 2023).The purpose of the present study is to get an optimal degradation value using appropriate doping with alkaline earth metals.

2. EXPERIMENTAL

2.1 Synthesis of Doped Manganites

$La_{0.7}Ca_{0.3}MnO_3$, $La_{0.7}Sr_{0.3}MnO_3$ and $La_{0.7}Ba_{0.3}MnO_3$ (hereafter will be called LCMO, LSMO and LBMO respectively) was synthesized via wet chemical method by mixing Sigma Aldrich-USA, AR grade $La(NO_3)_3.6H_2O$, $Ca(NO_3)_2.4H_2O$, $Sr(NO_3)_2$, $Ba(NO_3)_2$ and $Mn(NO_3)_2.4H_2O$ as the raw chemicals in 0.7:0.3:1.0 molar ratios. Stiochiometric amounts of all the salts were taken and separate solutions for each composition were made in de-ionized water. Citric acid was added in 100 % of total amount of the chemicals mixture solution for auto combustion followed by addition of 5 ml of ethylene glycol as surfactant. The prepared mixture with p^H adjusted to 8 was stirred vigorously for the next 30-45 min to get dark-brown gel. The viscous liquid so obtained was dried at 120 ^{0}C over night. The final powders $La_{0.7}A_{0.3}MnO_3$, (A= Ca, Sr and Ba) were calcined at 800 ^{0}C for 6 hours in the Muffle furnace (Model No: AI-106) to obtain manganites of nano dimensions..

2.2 Characterization Method

The structural, spectroscopic and optical properties of the synthesized powders were studied by X-Ray Diffraction (XRD), Inductively Coupled Plasma–Atomic Emission Spectroscopy (ICP–AES), Field Emission Scanning Electron Microscopy (FESEM), Fourier Transform Infrared Spectroscopy (FTIR) and UV–VIS absorption spectroscopy.

2.3 Photocatalytic Test

The photocatalytic degradation of aqueous MB solution (5 ppm, pH = 4) was carried out at room temperature separately by using LCMO, LSMO and LBMO as the photocatalysts (0.07 g l^{-1}),one 100 W fluorescent lamp as a visible-light source, 10 cm above the surface of MB solution at room temperature. At first, the mixture of water and prepared oxides were ultrasonicated for 15 minutes. The MB solution was added properly to each mixture with stirring at constant pH = 3.5, because the highest efficiency in the photocatalytic activity of the MB has been reported in acidic conditions (Afje and Ehsani, 2018; Behpour and Atouf, 2012); Khazaei et al., 2010). The reaction mixtures were allowed to be magnetically stirred in dark for 30 minutes with an aim to attain adsorption-desorption equilibrium of MB on the surface of the catalyst. In appropriate intervals, 5 mL of each suspension was collected and centrifuged. The MB concentration was determined by using the UV–VIS spectrophotometer for both the samples in the dark and after light irradiation. The

decreasing concentration of MB in the solution was used to investigate the activity of the LCMO, LSMO and LBMO particles.

3. RESULTS AND DISCUSSION

3.1 TG-DTA Analysis

Thermogravimetric studies of the prepared samples at the heating rates of 5 ^{0}C min^{-1} from 30 ^{0}C to 1000 ^{0}C, were carried out using HITACHI STA7200 thermal analyser. The curve showed that weight loss occurred in several steps. The primary weight loss found between 25^{0}C to 150 ^{0}C was associated with loss of water.(Fig. 1).

A minor disintegration was observed between 250 ^{0}C to 380 ^{0}C in all the cases of samples, appeared as notches which might have occurred due to breaking of polymeric chain. The second step weight loss between 400 ^{0}C to 570 ^{0}C appeared due to decomposition of nitrates and citrates and implied initial formation of nano-perovskite. The final stage of mass degradation took place between 600 ^{0}C to 800 ^{0}C which was attributed to the formation of phase pure or crystalline nano-perovskite. Above 800 ^{0}C there was a very weak mass degradation which showed completion of perovskite oxide phase formation. The result of TGA analysis could be used to estimate the calcinations temperature.

3.2 XRD Analysis

Powder XRD of the prepared $La_{0.7}Ca_{0.3}MnO_3$(LCMO), $La_{0.7}Sr_{0.3}MnO_3$(LSMO), $La_{0.7}Ba_{0.3}MnO_3$(LBMO) samples (Fig. 2) were carried out by X-ray diffractometer (PAN Analytical Empyrean Series 2) with Cu Kα (λ = 0.15406 nm) radiation in the range 2θ= 10^0-80^0 [Table-1], under current of 30 mA and 40 Kv. The synthesized samples have single-phase perovskite structures and it has been confirmed that there is no extra peak relating to the secondary phase. The most prominent peaks were obtained at 2θ value of 32.65^0, 32.71^0 and 32.40^0 for LCMO, LSMO and LBMO respectively along with other characteristic peaks confirming the crystal formations. There is a little variation in d-values in different samples which is attributed to distortion in crystal structures arising from change in bond lengths and bond angles. All strong peaks have small shift towards lower angle because of Ca, Sr and Ba due to incorporation of dopant ions into the lattice host material i.e. lanthanum manganite. The figure shows that the Ca, Ba, and Sr doped samples give characteristic broadened peaks which represent the smaller size of crystals in the compositions.The data were analyzed using a commercial X-pert package and FULLPROF program. The diffraction peaks matched with the X-pert high score PDF (code: 01-075-0440), indicating the formation of a cubic $LaMnO_3$perovskite phase.

It is observed that undoped $LaMnO_3$usually acquires an orthorhombic crystal structure. The diffraction peaks in the Ca doped composition are also indexed as an orthorhombic structure without any other secondary or impurity phase. However, the peaks in Sr and Ba doped compositions are indexed to the rhombohedral structure with the presence of minor impurity phases.

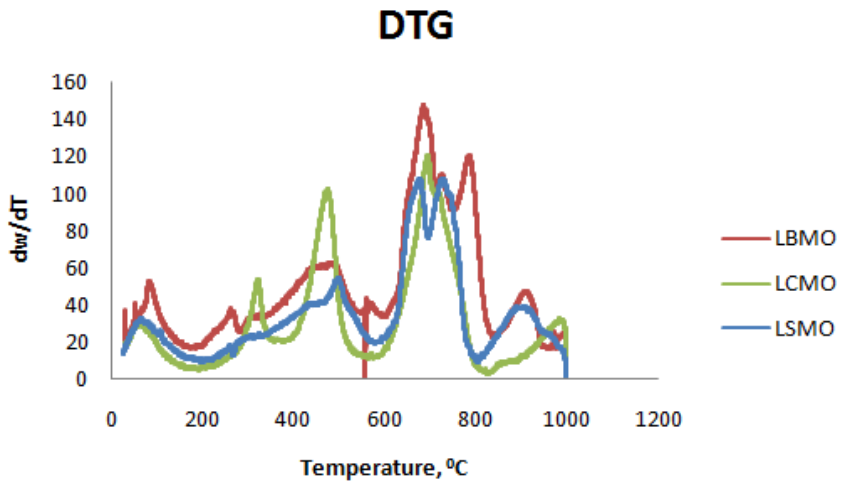

Fig. 1. Derivative Thermogravimetric curves of the perovskite samples

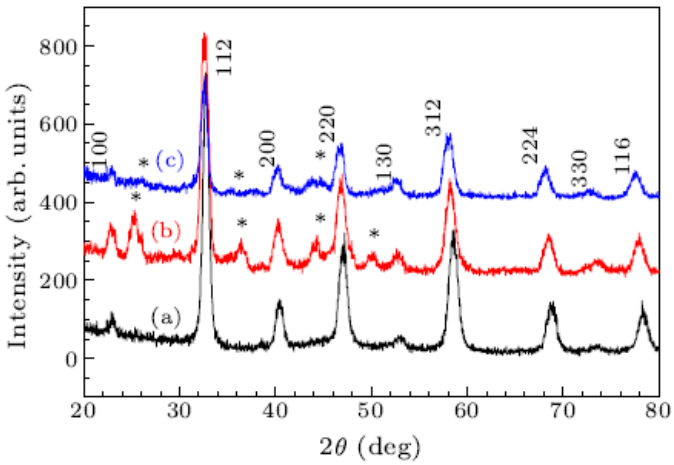

Fig. 2. XRD pattern of the nanoperovskite samples-(a):LCMO, (b):LSMO, (c):LBMO. The asterisks represent the $SrCO_3$ and $Ba(OH)_2$ impurities

Table 1. X- Ray Crystallographic data of nano-perovskite samples)

LCMO			LSMO			LBMO		
Pos. [°2θ]	**d-spacing [Å]**	**Rel. Int. [%]**	**Pos. [°2θ]**	**d-spacing [Å]**	**Rel. Int. [%]**	**Pos. [°2θ]**	**d-spacing [Å]**	**Rel. Int. [%]**
22.9058	3.88259	19.51	22.9243	3.8795	13.69	23.8733	3.7274	27.7
32.6502	2.74270	100.00	32.7176	2.7372	100	22.8307	3.8952	21.66
40.2325	2.24158	17.55	40.1473	2.2461	12.7	32.4006	2.7632	100
46.8260	1.94017	27.76	46.7879	1.9417	25.15	39.9911	2.25455	19.57
58.1931	1.58537	21.38	58.0691	1.58846	17.29	46.6222	1.94817	32.77
						57.9149	1.5923	24.72

The broadening of peak is because of the finite size of the crystals and broadening of peaks decreases with metal doping due to increase in grain size. Further, the post annealing temperature (800 °C for 6 h) removes all the impurities and develops pure phase nanoperovskites. The most intense peak (110) was used to calculate the crystallite size (D) by the equation $D = 0.9\lambda/\beta\cos\theta$, where $\lambda = 1.5405$ Å, the wavelength of incident X-ray, θ is the corresponding Bragg's diffraction angle and β is full width at half maxima of the (110) peak. Any secondary phase was not detected in XRD spectra which ensure the phase purity of the final product. Crystalline structure forms at a high-temperature treatment. As it can be seen from the DTG curves (Fig.2), the process of formation of crystalline nanoparticles is one-stage; it begins at 600 °C and finishes at 800 °C.

3.3 SEM Analysis

Morphological studies of the prepared sample were carried out using HITACHI S-3400N scanning electron microscope. The SEM pictures [Fig. 3] show that synthesized perovskite had spongy, irregular and rough surface with numerous cavities. The particles also had fluctuating sizes and shapes. This served to make sense of the great adsorptive characteristics.

FE-SEM images in Fig. 3 clearly showed that most of the grain sizes were distributed from 5 to 100 µm, which was much larger than one estimated by the Scherrer formula. This implied that our perovskite particles were polycrystalline. The presence of citric acid prevented agglomeration of the particles to a large extent (Khazaei et al., 2010). It was expected that large amount of gases evolved during calcination at high temperatures when citric acid decomposed. It was observed that undoped $LaMnO_3$ usually acquires an orthorhombic crystal structure.

3.4 EDAX Analysis

The Energy Dispersive Analysis X-ray (EDAX) study provided quantitative essential investigations of the atoms present on the surface of prepared samples (Fig. 4)**.**The related peaks in the spectrum are because of the

presence of La, Ca, Sr, Ba, Mn and O atoms. No extra impurity peaks were seen which affirmed that the synthesized sample was pure in nature. Likewise, the Atomic weight ratios of (La, M) :Mn, (M= Ca, Ba, Sr) were found to be 1.07,1.02 0.99 indicate the stoichiometric nature of the prepared samples. [Table-2]

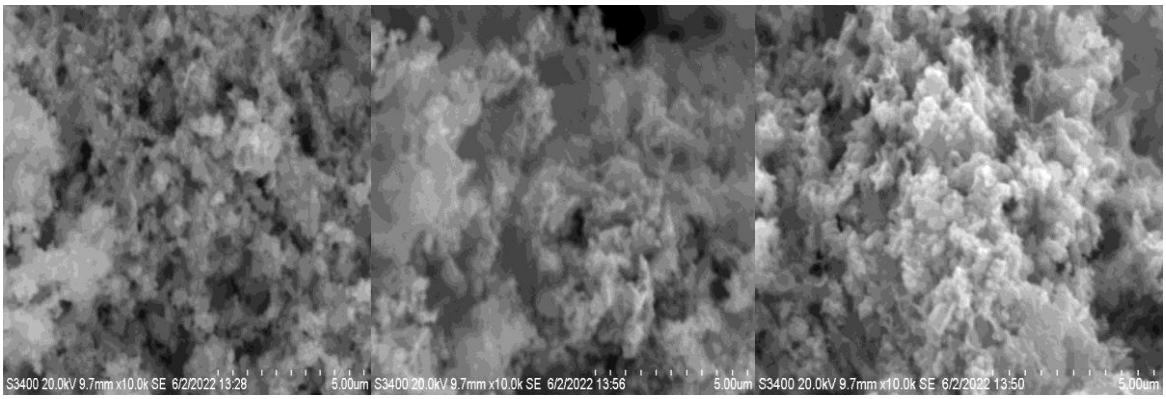

LBMO LSMO LCMO

Fig 3. Scanning Electron Microscopy photographs of the prepared samples

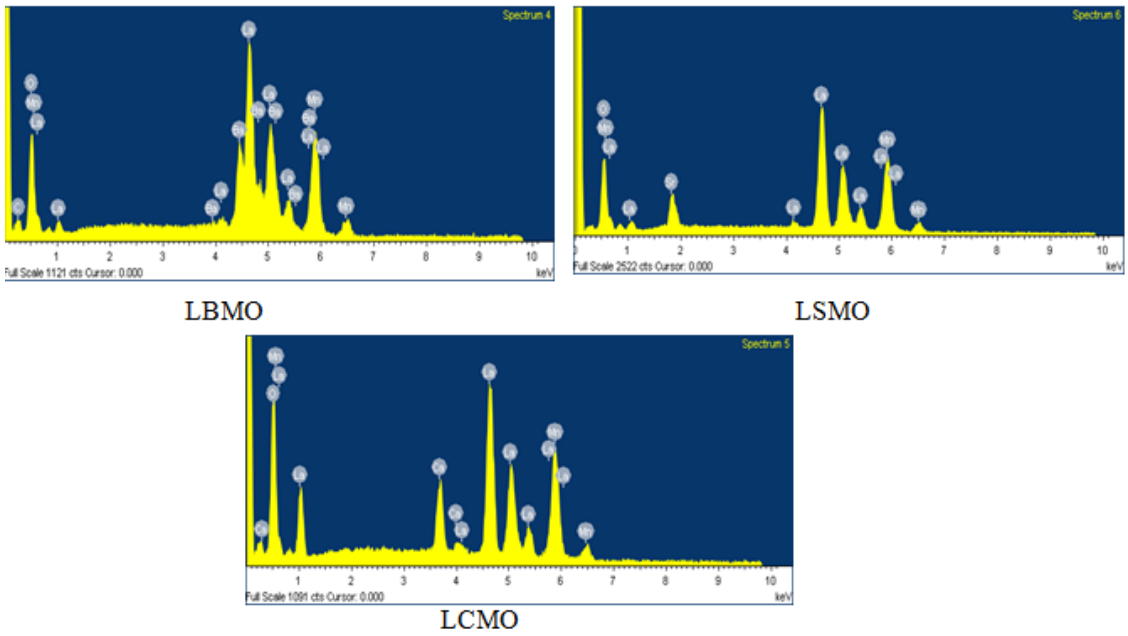

LBMO LSMO

LCMO

Fig.4. EDAX Patterns of synthesized LCMO; spectrum-5, LSMO; spectrum-4, & LBMO; spectrum-6

Table 2. EDAX elemental composition of synthesized samples

Element	Weight%	Atomic%	Element	Weight%	Atomic%	Element	Weight%	Atomic%
LCMO			**LBMO**			**LSMO**		
O K	13.73	50.57	O K	14.45	34.99	O K	14.66	44.67
Ca K	11.08	6.56	Mn K	25.42	27.89	Mn K	24.43	27.80
Mn K	23.77	22.85	Ba L	18.59	7.21	Sr L	12.69	6.95
La L	51.42	20.02	La L	40.11	21.43	La L	48.22	20.58
Totals	100.00	100.00		100.00	100.00		100.00	100.00

3.5 FT-IR Analysis

There is a complete similarity in FT-IR spectral pattern(Fig.5) of all the prepared samples without much variation in absorption data. The doped perovskites were analysed by using PERKIN ELMER UATR 2, FT-IR spectrophotometer. The LCMO spectra showed peaks at 492.94 cm^{-1}, 586.40 cm^{-1}, 880.59 cm^{-1}, 1060.90 cm^{-1}, 1160.37 cm^{-1} and 3609.33 cm^{-1} etc. LBMO perovskite sample shows absorption at 497.26cm^{-1}, 575.25cm^{-1}, 879.82cm^{-1}, 1145.16cm^{-1}, 3609.30cm^{-1}, etc. LSMO perovskite sample shows absorptions at 482.32cm^{-1}, 571.21cm^{-1}, 860.95cm^{-1}, 1058.07cm^{-1}, 1144.49cm^{-1}, 3608.82cm^{-1} etc. The main absorption bands around 492.94 cm^{-1}497.26 cm-1 and 482.32 cm^{-1} for LCMO, LBMO and LSMO respectively might have been due to the bending mode of Mn-O-Mn bond [Fig. 5]. The absorption band at 586.40 cm^{-1}, 575.25cm^{-1} and 571.21cm^{-1} arises from the stretching mode of Mn-O-Mn bond which involves motion of a change in Mn-O-Mn bond length. Thus the presence of both the peaks showed the strong metal-oxygen bond present in the sample. These two bands are related to the environment surrounding the MnO_6 octahedron in the ABO_3perovskite and confirms the formation of perovskite structure, which is in agreement with the XRD results. The peak at 880.59 cm^{-1}857.47cm^{-1} and 879.82cm^{-1} were due to the presence of atmospheric CO_2 whereas peaks at 1033.42 cm^{-1} and 1060.90 cm^{-1}1145.16cm^{-1}were due to the presence of little carbonates in the sample and these data are in conformity with other samples.. Besides, the peak around1450 cm^{-1} in case of all the samples are related to the asymmetric elongation of O-C-O vibration.

3.6 Optical Properties

The band gap energies of the doped perovskites were evaluated from the UV–VIS spectra by using the earlier methods (Afje and Ehsani, 2018). Considering the results of the band gap energy, the synthesized samples were found to be promising candidates for use in photocatalytic activities.The efficiency of photocatalytic degradation of the perovskite samples on MB dye was studied (Arabi et al., 2018; Hassan et al., 2022) with the help of eqn (1):

$$D\ \% = (A^0 - A) / A^0 \times 100 \quad (1)$$

where A^0 is the initial absorbance of MB solution and A shows the absorbance at time t.

The degradation efficiencies of the samples on organic dye(MB) over time intervals were represented in Table-3.

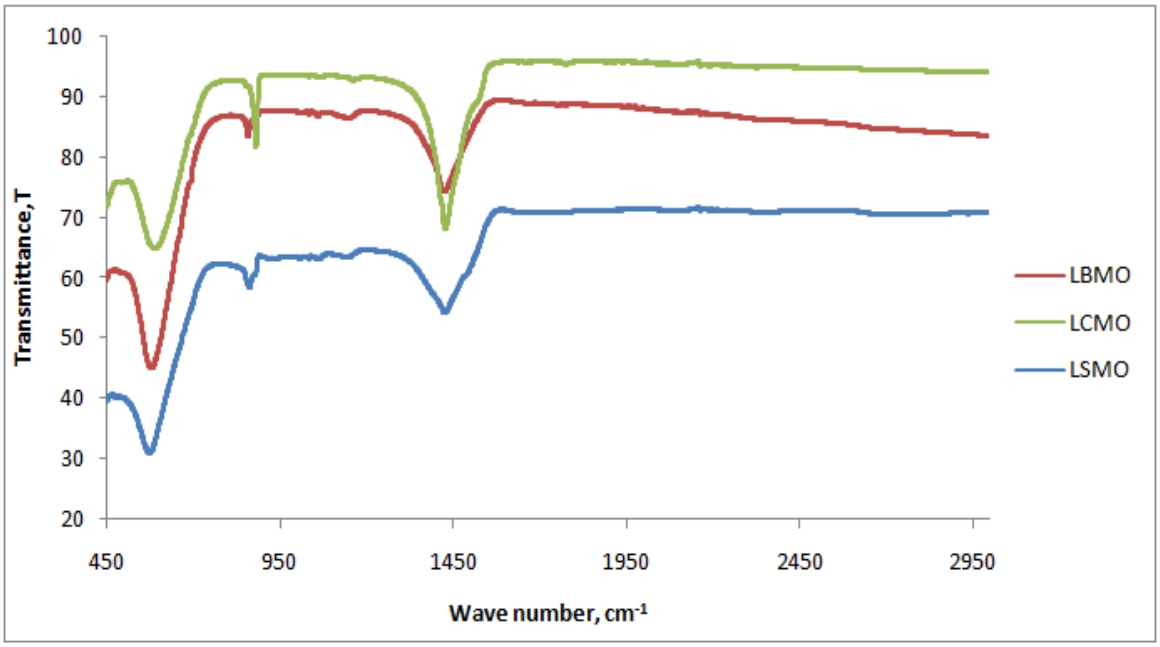

Fig.5. FT-IR spectral patterns of various prepared samples

Table 3. Percentage of Degradation of MB

	% Degradation in visible light		
Time, min	**LCMO**	**LBMO**	**LSMO**
0	52.07	35.42	42.06
20	59.07	38.79	44.53
40	60.70	41.68	47.64
60	63.61	42.32	48.47
80	66.01	44.58	52.01
100	68.52	47.92	54.87

The photocatalytic absorbance of MB of the different catalysts (LCMO, LBMO, and LSMO) at room temperature in visible light is shown in Fig.6a–c, respectively. For all the three samples, the maximum absorbance reveals at 675 nm wavelength and It was ascertained that the value decreases with increase in irradiation time in all the cases suggesting good photocatalytic activities of the prepared perovskites. Fig.6 shows photocatalytic absorbance of doped samples along with undoped one (LMO) after 100 min of irradiation. The figure indicated lowest absorbance in case of Ba doping and hence highest photocatalytic behaviours.The activity follow the order

LBMO > LSMO > LCMO > LMO.

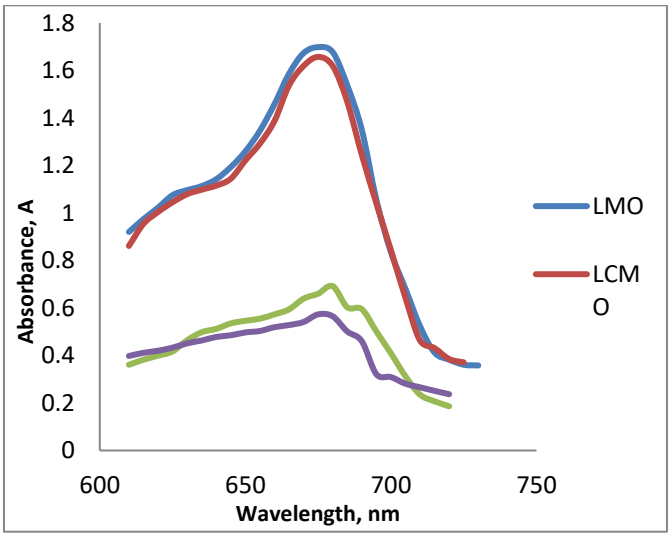

Fig. 6. Photocatalytic absorbance of prepared samples after 100 mins of irradiation

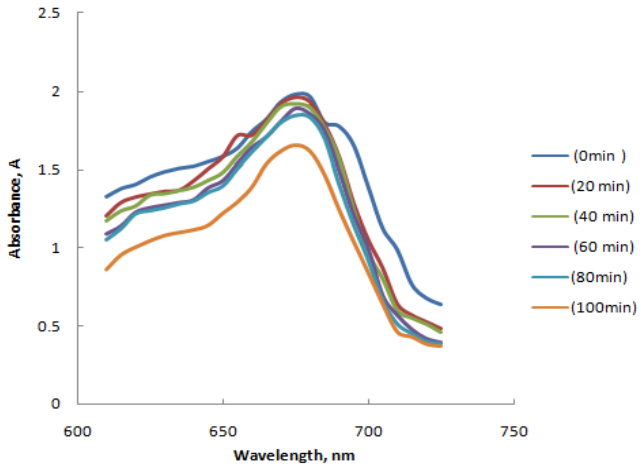

Fig. 6(a). Absorbance curves of MB at different time intervals using LCMO as catalyst

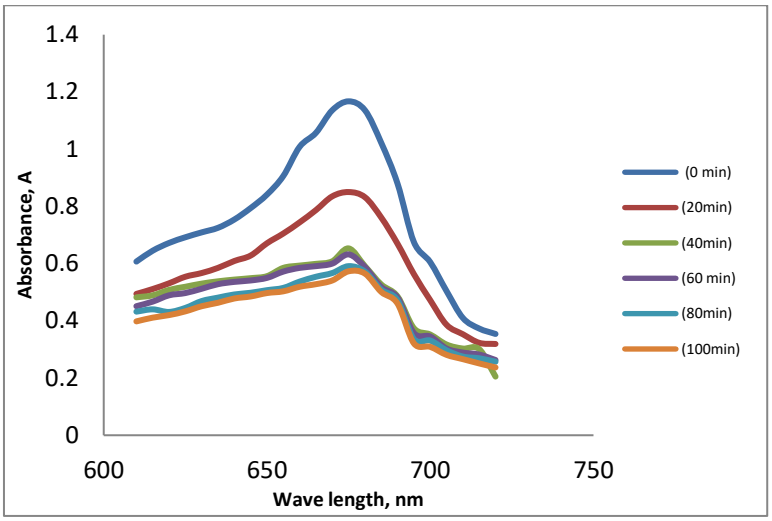

Fig. 6(b). Absorbance curves of MB at different time intervals using LBMO as catalyst

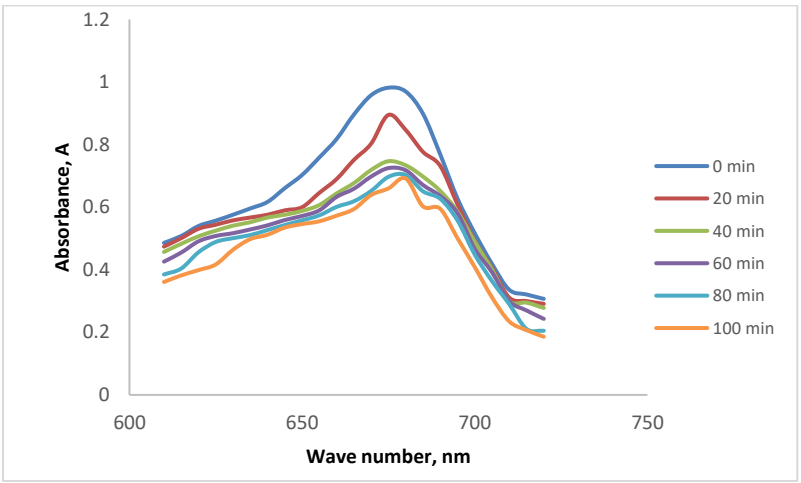

Fig. 6(c). Absorbance curves of MB at different time intervals using LSMO as catalyst

The absorbance of Dye (MB) solution decreased with increasing time of exposure to the light indicating the decrease in concentration and hence increase in degradation (Fig. 7). The percentage of degradation increased with irradiation time. However it was observed that highest rate of photodegradation was effected in 20 min of irradiation in case of 'Ca' whereas in case of 'Sr' and 'Ba' the time was 40 min. Fig. 7(a) shows the effect of irradiation time on photocatalytic degradation of methylene blue in all the cases. The decomposition steadily increased with time of irradiation up to 100 min and 68.52% of degradation was achieved in case of 'Ca' as dopant whereas for Sr and Ba the degradation percentage were 54.87% and 47.92% respectively. As the time of irradiation increased, the interaction of dye molecules increased with the surface of the photocatalyst thereby increasing the photodegradation efficiency (Lachheb et al., 2002; Baran et al., 2003; Akpan and Hameed, 2009). A shorter time interval 100 min was chosen in order to achieve faster rate of degradation within a short period of time.

3.7 Kinetics of Photodegradation

The kinetics and rate constants were analyzed with the help of Eq. 2 (Hussien et al., 2020; Hussien et al., 2020).

$$\ln(A/A^0) = -kt, \quad \text{.....} \quad (2)$$

where A^0 is the initial absorbance, A is absorbance after time t, and k is rate constant; the plot of $\ln(A/A^0)$ against the time t is linear according to Eq. 2.

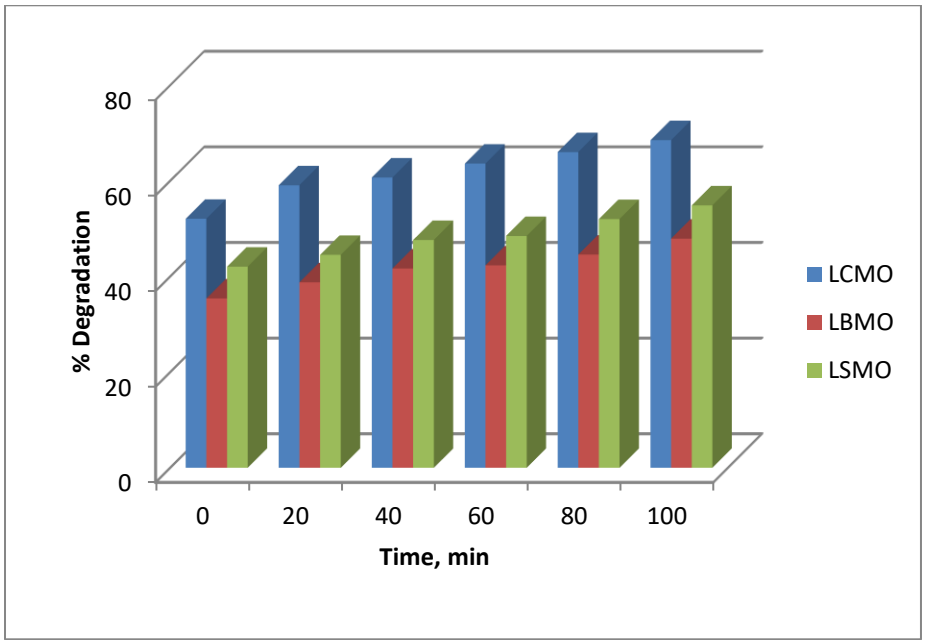

Fig. 7. Degradation percentage of Methylene Blue in presence of synthesized photocatalysts under visible light irradiation)

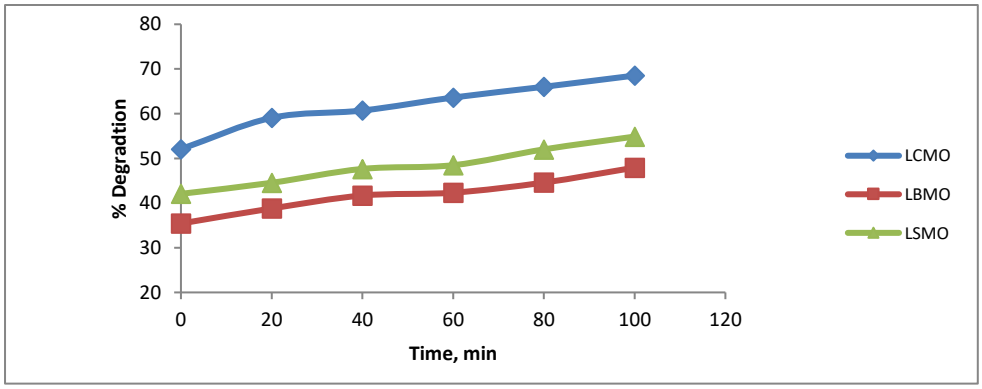

Fig. 7(a). Degradation percentage of Methylene Blue in presence of synthesized photocatalysts under visible light irradiation

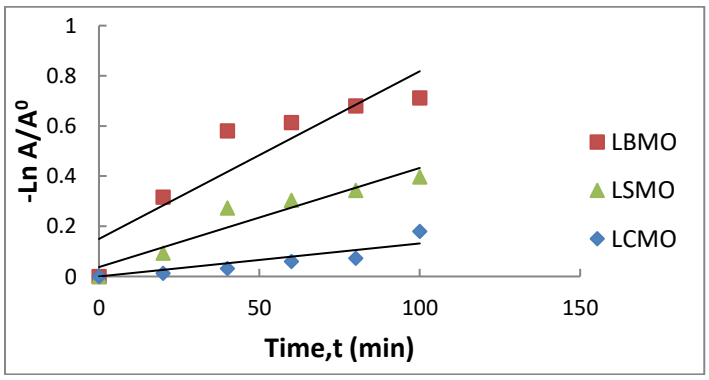

Fig. 8. Variation of ln A/A^0 with time 't' for the degradation kinetics using different perovskites as photocatalysts

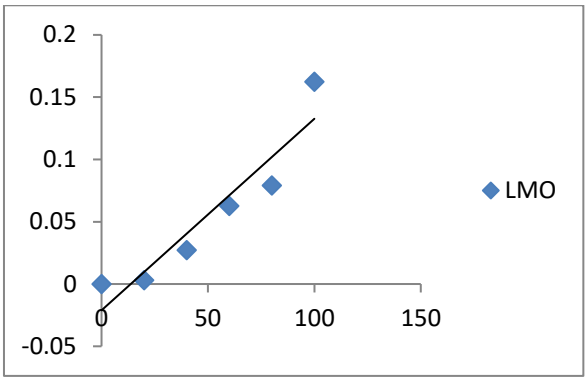

Fig. 8(a). Variation of ln A/A^0 with time 't' for the degradation kinetics using perovskite, LMO with no doping as photocatalysts

Thus, the values of 'k' were obtained directly from the slopes (Fig.8a) and was presented along with degradation efficiency after 100 mins of irradiation with visible light [Fig.9]. The 'k' values for the prepared perovskite samples were presented in Table-4.

Since the concentration of MB solution is directly proportional to the absorbance, the pseudo first order rate constant, k was estimated from the slopes of the linear plots (Fig. 8a). The linearity of the plots for definite MB concentrations, proved the applicability of the Langmuir–Hinshelwood equation for the photocatalytic degradation of MB.

By substituting La with a divalent M^{2+}cation, Mn^{4+}ions can be introduced into $LaMnO_3$(Akpanand Hameed, 2009). Since the parent sample ($LaMnO_3$) was Mn^{3+}-rich, $La_{1-x}M_xMnO_3$ ($La^{3+}{}_{1-x}M^{2+}{}_xMn^{3+}{}_{1-x}Mn^{4+}{}_xO_3$) with mixed-valence $Mn^{3+}$and Mn^{4+}played a major role inthe electronic structure of this sample. The catalytic activity of the investigated perovskites may be correlated with the presence of the active oxygen species (O^{2-}, $O_2^{\bullet-}$, O^-) determined by the structural defects generated due to high Mn^{4+}/Mn^{3+} ratio in the perovskite structure. Thus $La_{1-x}M_xMnO_3$ compound is called hole-doped manganite perovskites and the hole doping plays a role of shifting down to the Fermi level so that the conduction and valence band behaviour occurs (Hussien et al., 2020). Thus, the coexistence of electron and hole in manganites, introduce them as promising materials in optical devices.

Table4. Rate constant and degradation percentage of samples exposed to visible light after 100 mins

Perovskite Samples	% Degradation	Rate constant k, min^{-1}
LMO	42.63	0.001538
LCMO	68.52	0.001582
LSMO	54.87	0.003952
LBMO	47.92	0.006684

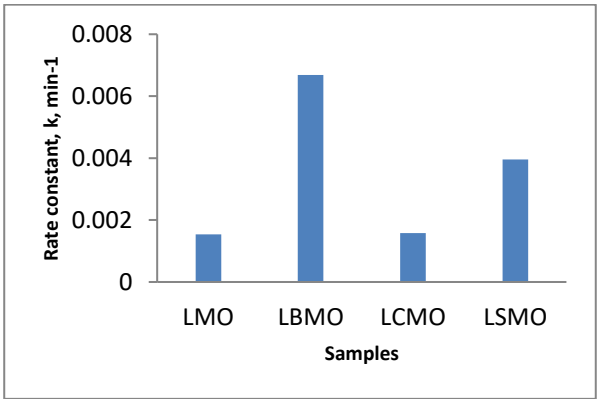

Fig. 9. Rate constants of degradation of MB using both doped and undopedperovskite samples

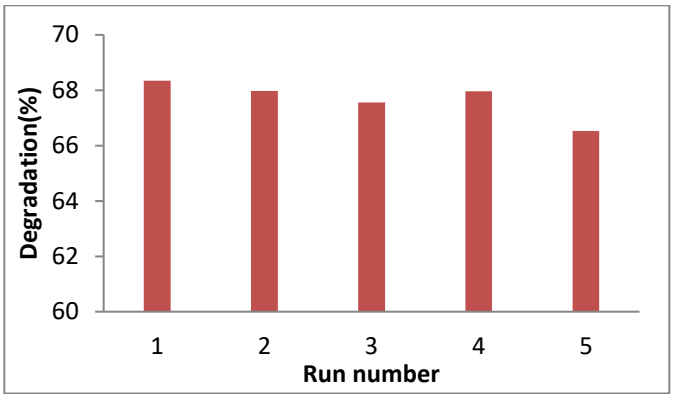

Fig. 10. Reusability of the LCMO sample

As well known, $OH^{\bullet}$ radicals degrade dye molecules into simpler compounds (CO_2 and H_2O). The impact of irradiation time on the percentage of dye degradation can be seen in Fig. 7a. Looking at the curves it is ascertained that the amount of degraded $OH^{\bullet}$ radicals increases with increasing irradiation time (Rahmayeni et al., 2020). The photo-degradation originated when the visible light irradiated the catalyst, so the photodegradation mechanism of dye solutions is based on the redox reactions for perovskite samples. The photon energy (*hu*) absorbed is equal to/or greater than the perovskite energy gap. During the photo excitation process, the valence band (VB) electron jumps to the conduction band (CB) and lets h+ on VB, which reacts with the adsorbed OH^- ions or the H_2O on the perovskite surface, producing $OH^{\bullet}$.

$hv + Catalyst \rightarrow e_{CB}^- + h_{VB}^+$ [i]
$H_2O \rightarrow H^+ + OH^-$ [ii]
$OH^- + h_{VB}^+ \rightarrow OH^{\bullet}$ [iii]
$e_{CB}^- + O_2 \rightarrow O_2^{\bullet -}$ [iv]
$O_2^{\bullet -} + H^+ \rightarrow HO_2^{\bullet}$ [v]
$2\ HO_2^{\bullet} \rightarrow 2H_2O_2 + O_2$ [vi]
$H_2O_2 \rightarrow 2\ OH^{\bullet}$ [vii]
$MB + OH^{\bullet} \rightarrow$ degraded product $+ H_2O + CO_2$ [viii]

Introduction on of Ca in to Lanthanum manganite has already been reported (Nayak and Padhi, 2023) which signified almost 68.52% of degradation after 100 mins of illumination with a pseudo first order rate constant of 1.582 x 10^{-3} min^{-1}. Introduction of larger cations (Sr, Ba) stabilizes the metallic state with an increased metal-insulator transition temperature. The introduction of a smaller cation (Ca) leads to an insulating state with increased resistivity attributed to the fact that smaller cationic size decreases the Mn-O-Mn bond angle and which in response decreases the double exchange(DE) mechanism between Mn-Mn ions(Khalid et al., 2013).

3.8 PhotocatalystReusability

The reusability of thesynthesizedsampleswere investigated by recycling the solidsamples after the photocatalyticdegradation under visible-light irradiation. The photocatalystswere collected after each run and washed with 0.01 MH_2SO_4solution and an excess amount of deionized water. In each run, the photocatalytic activity of thesolid sample was examined in the same condition as mentionedbefore up to 100 minutes and as shown in Fig. 10. The results showed thatthis material could retain its photocatalytic activity for at leastfive reaction cycles.

4. CONCLUSION

In this study $La_{0.7}Ca_{0.3}MnO_3$,$La_{0.7}Sr_{0.3}MnO_3$and $La_{0.7}Ba_{0.3}MnO_3$ nanoperovskite was synthesized by a simple Sol-Gel method followed by heat treatment at 800 ^{0}C. XRD showed that the obtained sample had perovskite structure. SEM showed micrometer sized randomly distributed crystal particles. Using Tauc's equation band gap energy values were found out which were in the range of photocatalytic activitiy with visible light irradiation. The photocatalytic activities were investigated by degradation of MB in aqueous solution under visible light irradiation which revealed efficient photocalytic activities. The photodegradation efficiency for decolorising MB solution (5 ppm) by using doped lanthanum manganite(0.07 g l^{-1}) after 100 min of illumination, was about 68.52 % , 54.87% and 47.92% respectively using Ca, Sr and Ba respectively. But reaction rate determination resulted in reverse trend with highest rate constant 6.684 x 10^{-3} min^{-1}in case of Ba doping..The result indicates that although Ba doping had best catalytic activity among the three, but with increase in time of irradiation Ca show highest degradability.

DISCLAIMER (ARTIFICIAL INTELLIGENCE)

Author(s) hereby declare that NO generative AI technologies such as Large Language Models (ChatGPT, COPILOT, etc) and text-to-image generators have been used during writing or editing of this manuscript.

COMPETING INTERESTS

Author has declared that no competing interests exist.

REFERENCES

Afje, F. R., & Ehsani, M. (2018).Size-dependent photocatalytic activity of $La_{0.8}Sr_{0.2}MnO_3$ nanoparticles prepared by hydrothermal synthesis. *Materials Research Express*, 5, 45012. https://doi.org/10.1088/2053-1591/aaba51

Akpan, U. G., & Hameed, B. H. (2009). Parameters affecting the photocatalytic degradation of dyes using TiO_2-based photocatalysts: A review. *Journal of Hazardous Materials*, 170, 520–529.

Anandan, K., Rajesh, K., Gayathri, K., Sharma, V. S., Hussain, S. G. M., &Rajendran, V. (2020). Effects of rare earth, transition and post transition metal ions on structural and optical properties and photocatalytic activities of zirconia (ZrO_2) nanoparticles synthesized via the facile precipitation process. *Physica E*, 124, 114342. https://doi.org/10.1016/j.physe.2020.114342

Arabi, A., Fazli, M., & Ehsani, M. (2018). Synthesis and characterization of calcium-doped lanthanum manganite nanowires as a photocatalyst for degradation of methylene blue solution under visible light irradiation. *Bulletin of Materials Science*, 41, 77. https://doi.org/10.1007/s12034-018-1590-6

Baran, W., Makowski, A., & Wardas, W. (2003). The influence of $FeCl_3$ on the photocatalytic degradation of dissolved azo dyes in aqueous TiO_2 suspensions. *Chemosphere*, 53, 87–95.

Barrocas, B., Sério, S., Rovisco, A., Nunes, Y., & Jorge, M. M. (2016). Removal of rhodamine 6G dye contaminant by visible light driven immobilized $Ca_{1-x}Ln_xMnO_3$ (*Ln* = Sm, Ho; 0.1 <*x*< 0.4) photocatalysts. *Applied Surface Science*, 360, 798–806.

Behpour, M., &Atouf, V. (2012). Study of the photocatalytic activity of nanocrystalline S, N-codopedTiO_2 thin films and powders under visible and sun light irradiation. *Applied Surface Science*, 258, 6595–6601.

Esmaeili, S., Ehsani, M. H., &Fazli, M. (2019).Structural, optical and photocatalytic properties of $La_{0.7}Ba_{0.3}MnO_3$ nanoparticles prepared by microwave method. *ChemPhys*, 529, 110576. https://doi.org/10.1016/j.chemphys.2019.110576

Ghozza, M. H., Yahia, I. S., & Hussien, M. S. A. (2023). Structure, magnetic, and photocatalysis of $La_{0.7}Sr_{0.3}MnO_3$ (*M* = Mn, Co, and Fe) perovskite nanoparticles: Novel photocatalytic materials. *Environmental Science and Pollution Research*, 30, 61106–61122. https://doi.org/10.1007/s11356-023-26411-9

Gowthami, K., Suppuraj, P., Thirunarayanan, G., Krishnakumar, B., Sobral, A. J. F. N., Swaminathan, M., &Muthuvel, I. (2018).$Fe_2V_4O_{13}$ assisted hetero-fenton mineralization of methyl orange under UV-A light irradiation. *Iran ChemCommun*, 6, 97–108.

Guillaume, P. L. A., Chelaru, A. M., Visa, M., &Lassine, O. (2018).Titanium oxide-clay as adsorbent and photocatalysts for wastewater treatment.*J MembrSciTechnol*, 8, 1000176. https://doi.org/10.4172/2155-9589.1000176

Hassan, A. E., Hussien, M. S. A., Elsayed, M. H., Mohamed, M. G., Kuo, S.-W., Chou, H.-H., Yahia, I. S., Wang, G., & Wen, Z. (2022). One-step construction of Y, C, and O tridoped $g\text{-}C_3N_4$ as a bifunctional photocatalyst for H_2 evolution and organic pollutant degradation under visible light irradiation. *Sustain Energy Fuels*, 6, 3858–3871.

Hussien, M. S. A., Mohammed, M. I., &Yahia, I. S. (2020). Flexible photocatalytic membrane based on *CdS/PMMA* polymeric nano composite films: multifunctional materials. *Environ SciPollut Res.*, 27, 45225–45237. https://doi.org/10.1007/s11356-020-10305-1

Hussien, M. S. A., Mohammed, M. I., &Yahia, I. S. (2020). Multifunctional applications of graphene-doped PMMA nanocomposite membranes for environmental photocatalytic.*J InorgOrganometPolym Mater.*, 30, 2708–2719. https://doi.org/10.1007/s10904-019-01433-4

Ichimura, K., Inoue, Y., &Yasumori, I. (1992).*Catal. Rev. Sci. Eng.*, 34, 301–320.

Ismail, D., Bahnemann, W., Robben, L., Yarovyi, V., &Wark, M. (2010).*Chem Mater*, 22, 108–116.

Isupova, L. A., Sutormina, E. F., Kulikovskaya, N. A., Plyasova, L. M., Rudina, N. A., Ovsyannikova, I. A., Zolotarskii, I. A., &Sadykov, V. A. (2005). *Catal. Today*, 105, 429–435.

Kanakaraju, D., & Wong, S. P. (2018).Photocatalytic efficiency of TiO_2-biomass loaded mixture for wastewater treatment. *J Chem*, 2018, ID 4314969. https://doi.org/10.1155/2018/4314969

Khalid, A., Siddiqi, S. A., &Aslam, A. (2013). Synthesis and Characterization of Alkaline-Earth Metal (Ca, Sr, and Ba) Doped Nano dimensional $LaMnO_3$ Rare-Earth Manganites. *Chin. Phys. Lett.*, 30, 077501. https://doi.org/10.1088/0256-307X/30/7/077501

Khazaei, M., Malekzadeh, A., Amini, F., Mortazavi, Y., & Khodadadi, A. (2010).Effect of citric acid concentration as emulsifier on perovskite phase formation of nano-sized $SrMnO_3$ and $SrCoO_3$ samples. *Cryst. Res. Technol.*, 45, 1064–1068.

Kim, J., Hwang, D. W., Kim, H. G., Bae, S. W., Lee, J. S., Li, W., & Oh, S. H. (2005). *Top.Catal.*, 35, 295–303.

Kumar, R. D., Thangappan, R., &Jayavel, R. (2018).Enhanced visible light photocatalytic activity of $LaMnO_3$ nanostructures for water purification.*Research on Chemical Intermediates*, 44, 4323–4337.

Kuo, J., & Kai, G. S. (2009).*Chin. Phys. B*, 18, 3035.

Lachheb, H., Puzenat, E., Houas, A., Ksibi, M., Elaloui, E., Guillard, C., & Herrmann, J. M. (2002).Photocatalytic degradation of various types of dyes (Alizarin S, Crocein Green G, Methyl Red, Congo Red, Methylene Blue) in water by UV-irradiated titania. *Appl. Catal. B: Environ.*, 39, 75–90.

Lago, R. M., Moura, F. C. C., Araujo, M. H., Ardisson, J. D., Macedo, W. A., & Albuquerque, A. S. (2007). *J. Braz. Chem. Soc.*, 18, 322–329.

Lee, Y. N., Lago, R. M., Fierro, J. L. G., Cortes, V., Sapina, F., & Martinez, E. (2001).*Appl. Catal. A*, 207, 17–24.

Nayak, H., & Padhi, B. (2023).Degradation of methylene blue using Ca-doped $LaMnO_3$ as a photocatalyst under visible light irradiation.*Results in Chemistry*, 6, 101104.https://doi.org/10.1016/j.rechem.2023.101104

Rahmayeni, R., Oktavia, Y., Stiadi, Y., Arief, S., &Zulhadjri, Z. (2020). Spinel ferrite of $MnFe_2O_4$ synthesized in *Piper betle* Linn extract media and its application as photocatalysts and antibacterial. *J Dispersion Sci Technol.*, 42, 1–10. https://doi.org/10.1080/01932691.2020.1721011

Sakamoto, M., Ahmed, T., Begum, S., &Huq, H. (2019). Water pollution and the textile industry in Bangladesh: flawed corporate practices or restrictive opportunities. *Sustainability*, 11, 1951. https://doi.org/10.3390/su11071951

Stephan, K., Hackenberger, M., Kiessling, D., & Wendt, G. (2004).*Chem. Eng. Technol.*, 27, 687–693.

Tao, S., Irvine, J. T. S., &Kilner, J. A. (2005).*Adv. Mater.*, 17, 1734–1737.

Yerkinova, A., Balbayeva, G., Inglezakis, V. J., &Poulopoulos, S. G. (2018).Photocatalytic treatment of a synthetic wastewater.*IOP Conf Series: Mater SciEng*, 301, 12143–12148. https://doi.org/10.1088/1757-899X/301/1/012143

Yi, N., Cao, Y., Su, Y., Dai, W. L., He, H. Y., & Fan, K. N. (2005). *J. Catal.*, 230, 249–253.

Zhou, Y., Zhu, X., & Li, S. (2018). Effect of heat treatment condition on magnetic, electrical transport and magneto resistance properties of $La_{0.67}Sr_{0.33}MnO_3$ manganite coatings.*Ceramics International*, 44, 15010–15018.

Peer-review history:
The peer review history for this paper can be accessed here:
https://pr.sdiarticle5.com/review-history/135080